UDC 54.05+546.02

DOI: 10.15372/CSD2019134

Low-Temperature Mechanochemical Synthesis of Zinc-Substituted Hydroxyapatite

N. V. BULINA, M. V. CHAIKINA, O. B. VINOKUROVA, I. YU. PROSANOV, N. Z. LYAKHOV

Institute of Solid State Chemistry and Mechanochemistry, Siberian Branch of the Russian Academy of Sciences, Novosibirsk, Russia

E-mail: bulina@solid.nsc.ru

Abstract

Results of the investigation of the structure of zinc-substituted hydroxyapatite formed during low-temperature solid phase mechanochemical synthesis are presented. It is shown that a single-phase zinc-substituted hydroxyapatite with a degree of substitution of up to 0.4 mol zinc ions per 1 mol of hydroxyapatite is formed in a planetary ball mill AGO-2 after 30 min of mechanical impact on the mixture of initial reagents ($CaHPO_4$, CaO, $Zn(H_2PO_4)_2 \cdot 2H_2O$). Two types of substitution reactions for zinc ions were studied: the substitution of calcium ions and hydroxide ions. The dynamics of lattice parameters of the synthesized samples showed that zinc ions most probably occupy the positions of calcium ions in the course of mechanochemical synthesis. After high-temperature treatment, the positions of zinc ions change: they are moved into the hydroxyl channel on the *c* axis, displacing OH groups and forming O–Zn–O chains elongated along the *c* axis. The limit of substitution, in this case, is reduced to 0.2 mol of zinc per 1 mol of hydroxyapatite. The synthesized samples may be used to obtain medical bioresorbable hardware and coatings with antibacterial properties.

Keywords: mechanochemical synthesis, hydroxyapatite, substitution, zinc

INTRODUCTION

Hydroxyapatite (HAP) $Ca_{10}(PO_4)_6(OH)_2$ is widely used in various areas of medicine: in traumatology and orthopedy, craniofacial surgery and dentistry, in therapy and cosmetology, as a tool for targeted drug delivery. It serves as a material for biocompatible ceramic products, composites, fillers of bone defects, medicinal cements and coatings of implants [1–3].

Hydroxyapatite is characterized by the hexagonal crystal system with space group $P6_3/m$ [1]. The uniqueness of the apatite structure is in a very broad possibility of substitutions and the formation of solid solutions. In this connection, organogenic HAP has a more complicated composition in comparison with that presented above, including a number of substitutions in the anion and cation sublattices playing an essential biological role [4, 5]. All ions in the HAP lattice are subjected to substitution; both isovalent and heterovalent substitution for the ions of other chemical elements or their groups is possible [6].

Substitutions in HAP structure change its physicochemical and biological properties substantially. For instance, the introduction of zinc, which is a bactericide element, renders antibacterial properties to HAP, which promotes the prevention of inflammation [6]. Due to this important feature, HAP is used as a component in the coatings of implants, in biocompatible ceramics and composites for medical properties [7, 8].

The synthesis of zinc-substituted hydroxyapatite (Zn-HAP) was extensively described in the literature [9–22]. However, the problem of the structure of the formed apatite, namely localization of zinc ions, remains controversial. According to the data of the authors of [19], Zn^{2+} occupies the vacancies of Ca^{2+} in Ca(2) positions in defect-bearing complexes at the stage of the formation

of Zn-HAP structure. The concentration of vacancies in Ca-deficient apatite is less than 0.1 mol per 1 mol of HAP, so the substitution of Ca^{2+} by Zn^{2+} is also limited by several molar percent [19]. The authors of [16] concluded that the localization of Zn ions in the position of Ca(2) is more favorable energetically than in Ca(1) position. In this case, zinc has the tetrahedral surrounding, where one of the four oxygen ions directly bound with zinc is from the nearest hydroxyl group, and the other three are from the neighbouring phosphate groups. This arrangement of the ions explains a decrease in the HAP unit cell parameter *a* from 9.488 to 9.319 Å, because the hydroxyl group shifts from its position at the *c* axis moving closer to the zinc ion, which in its turn shifts from the Ca(2) position towards the hydroxyl group. The authors of [17] demonstrated that Zn-HAP is formed after the introduction of up to 0.2 mol of zinc ion per 1 mol of HAP. With higher concentrations of the added dopant, other calcium-zinc phosphate compounds are formed. It was detected that the lattice parameters of the samples decrease while the concentration of the introduced Zn reaches 10 mol. %, and then they increase. According to the X-ray structural data described in [10], lattice parameters *a* and *c* decrease until the concentration of the introduced Zn^{2+} reaches 10 mol. %, and at 15 mol. % parameter *a* starts to increase, while *c* remains unchanged.

An interesting point of view was presented in [20–22]: the authors suppose than Zn^{2+} may enter HAP structure in the position of OH^- located at *c* axis, with the formation of O–Zn–O chains. Depending on the amount of introduced Zn and the temperature of sample annealing, the amount of zinc incorporated into HAP structure, its position and the number of the formed phases change. Under the conditions of the sol-gel synthesis of Zn-HAP, the substitution of calcium ions was not observed either in the first position or in the second one. According to the data of the authors of [21], after annealing at 500 °C the samples are monophase, and the insertion of Zn^{2+} into HAP structure is not detected. With an increase in annealing temperature to 600 °C, β-tricalcium phosphate (β-$Ca_3(PO_4)_2$) appears; its content after annealing at 900 °C is maximal. Zinc ions partially substitute calcium ions in the structure of β-$Ca_3(PO_4)_2$ in the positions of Ca(4) and Ca(5). A small amount of Zn^{2+} enters the hexagonal channel of the structure of Zn-HAP described by the formula $Ca_{10}Zn_x(PO_4)_6(OH)_{2-2x}O_{2x}$, where $x = 0.07$ for the case when annealing is carried out at 800 °C. With an increase in sample annealing temperature, the amount of Zn^{2+} in the structure increases, and at the maximal substitution obtained by the authors of [21], the composition of Zn-HAP is described by the formula: $Ca_{10}Zn_{0.26}(PO_4)_6O_{0.52}(OH)_{1.48}$.

The goal of the present work was to investigate the possibility of the synthesis of Zn-HAP using the mechanochemical method and to analyze the structure of the obtained compounds.

EXPERIMENTAL

Mechanochemical synthesis (MCS) of the samples was carried out in the AGO-2 planetary mill [23] in two water-cooled steel jars 150 mL in volume, with steel balls with the total mass 200 g, at the frequency of jar rotation around the axis 1800 r.p.m. The ratio of the portion of the reaction mixture to the ball mass was 1 : 20. Before synthesis, the preliminary lining of the working zone of the mill by the reaction mixture with the same composition was carried out. According to the data of atomic absorbtion analysis, iron content in samples after MCS did not exceed 0.05 mass %.

Initial components for the synthesis of Zn-HAP were anhydrous calcium hydroorthophosphate $CaHPO_4$ (pure Ch. reagent grade), annealed calcium oxide CaO (pure Ch. reagent grade), and monosubstituted zinc phosphate dihydrate $Zn(H_2PO_4)_2 \cdot 2H_2O$ (analytically pure reagent grade, Ch.D.A.). According to the certificates of these reagents, the concentrations of the main impurities (sulphates and iron) did not exceed 0.03 mass %. These concentrations may have only a positive effect on the biological properties of the material to be synthesized [6].

The synthesis of Zn-HAP samples with different concentrations of zinc ions was carried out according to reactions shown in Table 1. In the samples St-0.2Zn and St-0.4Zn, the substituent was introduced relying on the assumption that zinc ions substitute calcium ions (within the stoichiometry), while in the samples aSt-0.2Zn and aSt-0.4Zn – hydroxide ions (above the stoichiometry).

The synthesized samples were annealed at a temperature of 1000 °C for 2 h in a PVK 1.4-8 electric furnace (Russia) at a rate of 10 °C/min.

The samples after MCS and after annealing were investigated by means of X-ray structure analysis and IR spectroscopy. X-ray diffraction patterns were recorded with a powder diffrac-

TABLE 1
Reactions of the mechanochemical synthesis of Zn-HAP samples

Sample	Reaction No.	Reaction
St-0.2Zn	1	$5.6CaHPO_4 + 4.2CaO + 0.2Zn(H_2PO_4)_2 \cdot 2H_2O \longrightarrow Ca_{9.8}Zn_{0.2}(PO_4)_6(OH)_2 + nH_2O$
St-0.4Zn	2	$5.2CaHPO_4 + 4.4CaO + 0.4Zn(H_2PO_4)_2 \cdot 2H_2O \longrightarrow Ca_{9.6}Zn_{0.4}(PO_4)_6(OH)_2 + nH_2O$
aSt-0.2Zn	3	$5.6CaHPO_4 + 4.4CaO + 0.2Zn(H_2PO_4)_2 \cdot 2H_2O \longrightarrow Ca_{10}(PO_4)_6(OH)_{1.6}(ZnO_2)_{0.2} + nH_2O$
aSt-0.4Zn	4	$5.2CaHPO_4 + 4.8CaO + 0.4Zn(H_2PO_4)_2 \cdot 2H_2O \longrightarrow Ca_{10}(PO_4)_6(OH)_{1.2}(ZnO_2)_{0.4} + nH_2O$

tometer Bruker D8 Advance (Germany) in Bragg–Brentano geometry with CuK_α radiation. X-ray phase analysis of the compounds was carried out using the ICDD PDF-4 database of powder diffraction patterns (2011). Refinement of unit cell parameters, crystallite size, and calculation of phase concentrations were carried out according to Rietveld method using a Topas 4.2 software (Bruker, Germany). IR spectra were recorded with an Infralyum-801 spectrometer (Russia), samples were analyzed in the form of tablets that were prepared by pressing with KBr powder.

RESULTS AND DISCUSSION

The diffraction patterns of the samples after MCS are shown in Fig. 1, *a*. One can see that all the samples are identical; only the reflections of HAP phase are present (card PDF [10-73-8417]), which points to the monophase nature of the resulting substances. The value of lattice parameter *a* for Zn-HAP and unsubstituted HAP is the same, while parameter *c* decreases with an increase in the concentration of the introduced Zn^{2+} (Table 2). The average crystallite size is within the nanometer range and equals 20–24 nm. The radius of Zn^{2+} (0.74 Å) is substantially smaller than the radius of Ca^{2+} (0.99 Å), so it may be assumed that zinc ions substitute calcium ions during MCS leading to a decrease in parameter *c*.

The IR spectra of the samples after MCS obtained according to reactions (1)–(4) (see Table 1) are identical (see Fig. 1, *b)*. The basic absorption bands of the phosphate group of HAP (570, 602 cm^{-1}), hydroxyl group of HAP (630, 3573 cm^{-1}), carbonate group incorporated into HAP structure (1427, 1490 cm^{-1}) are present, and a broad band of sorbed water released during the synthesis is observed (3000–3700 cm^{-1}). These correspond to the absorption bands of unsubstituted HAP synthesized using the same method [24].

It follows from the above-mentioned data that nano-sized HAP crystallites formed during MCS contain CO_3^{2-} and sorbed water. Zinc ions are likely to be localized in the positions of calcium ions and possibly in crystal defects because the samples are poorly crystallized, with HAP crystallite size less than 30 nm.

After annealing, the diffraction patterns of the samples of St series (reactions (1)–(2)) contain the reflections of the β-$Ca_3(PO_4)_2$ phase in addition to HAP reflections (Fig. 2, *a*), while for the St-0.4Zn sample also the reflections of ZnO are

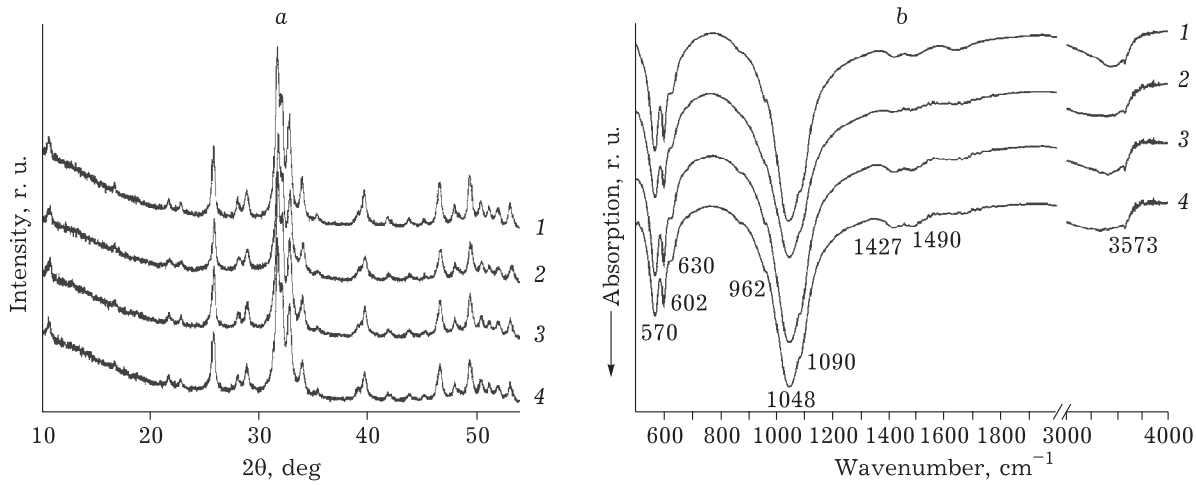

Fig. 1. Diffraction patterns (*a*) and IR spectra (*b*) of Zn-HAP samples after synthesis according to reactions (1)–(4) (*1–4*, respectively). For designations, see Table 1.

TABLE 2

Phase composition and lattice parameters of HAP phase

Sample	Composition	HAP lattice parameter, Å		Crystallite size, nm
		a	*c*	
	MCS			
HAP*	100 % HAP	9.433(1)	6.893(1)	24(1)
St-0.2Zn	100 % HAP	9.432(2)	6.885(1)	24.0(2)
St-0.4Zn	100 % HAP	9.430(2)	6.881(2)	19.5(4)
aSt-0.2Zn	100 % HAP	9.430(2)	6.888(2)	21.3(2)
aSt-0.4Zn	100 % HAP	9.426(2)	6.886(2)	21.3(4)
	Annealing			
HAP*	99.5 % HAP+0.5 % CaO	9.42095(3)	6.88103(3)	225(22)
St-0.2Zn	92 % HAP + 8 % $Ca_3(PO_4)_2$	9.4177(2)	6.8940(2)	156(3)
St-0.4Zn	84.5 % HAP + 15 % $Ca_3(PO_4)_2$ + 0.5 % ZnO	9.4153(3)	6.8975(2)	152(3)
aSt-0.2Zn	100 % HAP	9.4210(2)	6.8936(2)	210(4)
aSt-0.4Zn	99.3 % HAP + 0.7 % ZnO	9.4212(2)	6.8932(2)	185(4)

Note. Here and in Table 3 the standard deviations of the values under refinement are given in parentheses.
* Data from [24].

observed. The appearance of the β-$Ca_3(PO_4)_2$ phase in the annealed samples points to the fact that MCS leads to the formation of calcium-deficient hydroxyapatite (CDHAP), in which a phase transition is observed at a temperature of ~800 °C, proceeding with the formation of HAP and β-$Ca_3(PO_4)_2$ [25]. The lack of Ca ions in the structure of HAP obtained according to reactions (1) and (2) may be observed in the case if Zn ions do not occupy the positions of Ca ions. Then, relying on the literature data [20–22], we may assume that zinc ions are localized in the structure of HAP at the *c* axis occupying the positions of hydroxide ions and forming the chains O–Zn–O. In this case, the corresponding changes in the lattice should be observed: a decrease in parameter *a* and an increase in *c* [20, 22]. The comparison of lattice parameters of annealed Zn-HAP and HAP samples (Table 2) shows that exactly this dynamics is observed. In addition, the parameters of the β-$Ca_3(PO_4)_2$ phase increase with an increase in the concentration of the introduced zinc ions (Table 3), therefore, substitution also occurs in β-$Ca_3(PO_4)_2$. The presence of 0.5 mass % ZnO in the sample St-0.4Zn points to the low substitution limit in HAP and β-$Ca_3(PO_4)_2$. The authors of [22] showed that the substitution of OH^- by Zn^{2+} in the HAP structure starts at a temperature of ~900 °C. In our case, this type of substitution also is not observed in MCS samples before annealing.

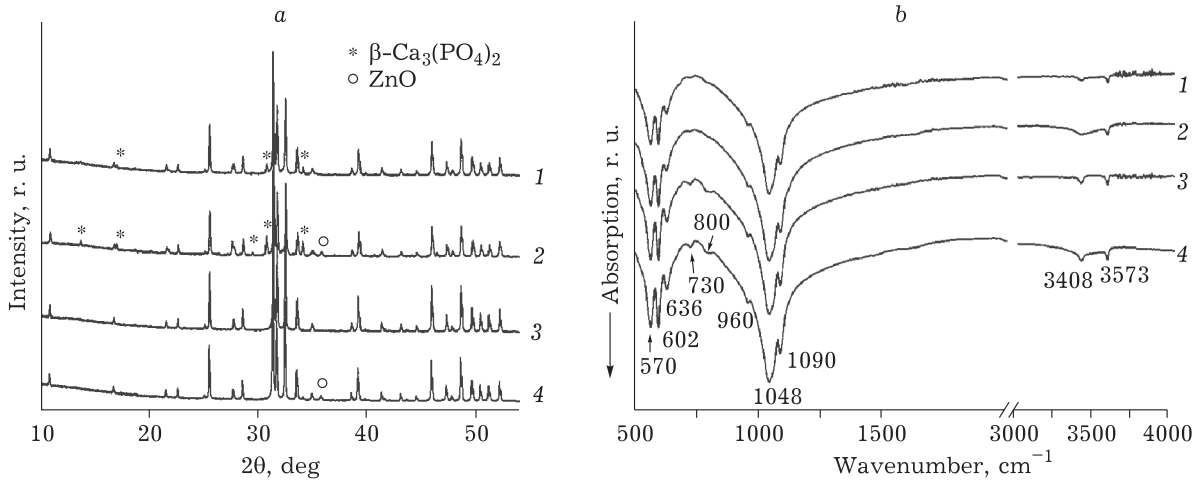

Fig. 2. Diffraction patterns (*a*) and IR spectra (*b*) of Zn-HAP samples according to reactions (1)–(4), annealed at a temperature of 1000 °C (*1*–*4*, respectively). For designations, see Table 1.

TABLE 3

Lattice parameters of the β-$Ca_3(PO_4)_2$ in annealed samples

Sample	Lattice parameters β-$Ca_3(PO_4)_2$, Å		Crystallite size, nm
	a	*c*	
St-0.2Zn	10.3632(12)	37.3031(80)	134(20)
St-0.4Zn	10.3825(8)	37.3284(40)	170(16)

Note. See Table 2.

A different situation is observed in the samples of the aSt series after annealing. The aSt-0.2Zn sample is monophase, while aSt-0.4Zn contains 0.7 mass % ZnO. The presence of only one phase in the aSt-0.2Zn sample synthesized according to reaction (3) confirms the assumption that zinc ions are localized at the *c* axis, and the presence of ZnO in the sample aSt-0.4Zn points to the fact that the substitution limit is within the range $0.2 < x < 0.4$ mol of zinc ion per 1 mol of HAP. It was demonstrated in [20] that the substitution limit for Zn-HAP samples obtained using the sol-gel method is 0.26 mol of zinc ions per 1 mol of HAP. So low substitution limit may be explained by the fact that the presence of the ions of different types along the 6_3 axis of HAP structure, where hydroxide ion is usually localized, leads to strong distortions in the Zn-HAP lattice.

The IR spectra of the samples after annealing and after MCS are strongly different from each other (see Fig. 1, *b* and 2, *b*). The absorption bands of the phosphate group did not change their position in the samples after annealing, while changes are observed for the absorption bands of OH groups. In the region of the stretching vibrations of hydroxide ion, a new band with the wavenumber of 3408 cm^{-1} is present. The authors of [20] suppose that zinc ion, substituting the hydroxide ion, is localized between two oxygen ions in the form of an O–Zn–O group extended along the *c* axis. Oxygen ions bound with zinc shift just above from their positions and occupy the position in the plane of calcium ions. As a result of this shift, the distance between hydroxide ions and oxygen ion decreases, which leads to the formation of a new hydrogen bond; an absorption band with the wavenumber of 3408 cm^{-1} appears in the IR spectrum. The frequency of libration vibrations of OH group increases in this situation (636 instead of 630 cm^{-1} for HAP). In addition, new absorption bands appear at 730 and 800 cm^{-1}; these bands may be attributed to the vibrations of O–Zn–O group [26].

CONCLUSION

Monophase nanocrystalline Zn-HAP with substitution degree 0.2 and 0.4 mol of zinc ions per 1 mol of HAP was synthesized by means of low-temperature solid-phase mechanochemical synthesis through activation for 30 min in a planetary mill. The simplicity of the synthesis method and the high substitution degree are the advantages of this method in comparison with other methods of obtaining Zn-HAP (described above). It was revealed that the insertion of zinc ions in mechanochemically synthesized samples causes a decrease in lattice parameter *c*, which is connected, most probably, with the localization of zinc ions in the positions of calcium ions. During the high-temperature annealing of mechanochemically synthesized samples, zinc ion changes its position in HAP structure: it substitutes the hydroxide ion at the *c* axis. This position of zinc ion may be more advantageous during annealing. It was established that a substantially higher substitution degree is possible in the mechanochemically synthesized samples than in the annealed ones. The MCS method allows solving the problem of obtaining Zn-HAP with a high degree of substitution on an industrial scale with the outlooks for further application in medicine to make bioresorptive products and coatings.

Acknowledgements

The investigation was carried out with financial support from the RFBR within the research project No. 18-29-11064.

REFERENCES

1 Elliott J. C., Structure and Chemistry of Apatite and Other Calcium Orthophosphates, Amsterdam, Elsevier, 1994. 371 p.
2 Barinov S. M., Komlev V. S., Bioceramics Based on Calcium Phosphates [in Russian], Moscow, Nauka, 2005. 201 p.
3 Dorozhkin S. V., *J. Funct. Biomater.*, 2010, Vol. 1, P. 22–107.
4 Boskey A. L., *Bonekey Rep.* [Electron. J.], 2013, No. 2, Article number: 447. URL: https://www.ncbi.nlm.nih.gov/ pmc/articles/PMC3909232/ (accessed 10.05.2019).
5 Liu Q., Huang S., Matinlinna J.P., Chen Z., Pan H., *BioMed Research International.*, 2013, Vol. 2013, Article ID 929748. URL: https://www.hindawi.com/journals/bmri/2013/929748/abs/ (accessed 10.05.2019).
6 Šupová M., *Ceram. Int.*, 2015, Vol. 41, P. 9203–9231.
7 Begama H., Nandi S. K., Chanda A., Kundu B., *Research in Veterinary Science,* 2017, Vol. 115, P. 1–9.
8 Thian E. S., Konishi T., Kawanobe Y., Lim P. N., Choong C., Ho B., Aizawa M., *J. Mater. Sci.: Mater. Med.*, 2013, Vol. 24, P. 437–445.

9 Saxena V., Hasan A., Pandey L. M., *Materials Technology*, 2018, Vol. 33, No. 2, P. 1–13.
10 Suchita K., Uma B., Seema K., *Asian J. Eng. Appl. Technol.*, 2014, Vol. 3, No. 2, P. 63–67.
11 Iqbal N., Kadir M. R. A., Mahmood N. H., Salim N., Froemming G. R. A., Balaji H. R., Kamarul T., *Ceramics International*, 2014, Vol. 40, P. 4507–4513.
12 Fadeeva I. V., Bakunova N. V., Komlev V. S., Medvetskiy L., Fomin A. S., Gurin A. N., Barinov S. M., *Dokl. AN*, 2012, Vol. 442, No. 6, P. 780–783.
13 Montoya-Cisneros K. L., Rendón-Ángeles J. C., Matamoros-Veloza Z., Yanagisawa K., *Mat. Lett.*, 2017, Vol. 195, P. 5–9.
14 Zhang H., Zhao C., Wen J., Li X., Fu L., *Ceramics-Silikáty*, 2017, Vol. 61, No. 3, P. 244–249.
15 Zhao X., Zhu Y., Zhu Z., Liang Y., Niu Y., Lin J., *J. Chem.* [Electron. J.], 2017, Vol. 2017, 4619159. URL: https://www.hindawi.com/journals/jchem/2017/4619159/ abs/ (accessed 10.05.2019).
16 Tang Y., Chappell H. F., Dove M. T., Reeder R. J., Lee Y. J., *Biomaterials*, 2009, Vol. 30, P. 2864–2872.
17 Ren F., Xin R., Ge X., Yang L., *Acta Biomaterialia*, 2009, Vol. 5, P. 3141–3149.
18 Sopyan I., Gunawan G, Shah Q. H., Mel M., *Materials and Manufacturing Processes*, 2015, Vol. 31, P. 713–718.
19 Matsunaga K., Murata H., Mizoguchi T., Nakahira A., *Acta Biomaterialia*, 2010, Vol. 6, P. 2289–2293.
20 Gomes S., Nedelec J. M., Jallot E., Sheptyakov D., Renaudin G., *Chem. Mater.*, 2011, Vol. 23, P. 3072–3085.
21 Gomes S., Nedelec J. M., Renaudin G., *Acta Biomaterialia*, 2012, Vol. 8, P. 1180–1189.
22 Renaudin G., Gomes S., Nedelec J. M., *Materials*, 2017, Vol. 10, P. 92.
23 Patent SU 975068, 1982.
24 Bulina N. V., Chaikina M. V., Prosanov I. Y., Dudina D. V., Solovyov L. A., *J. Solid State Chem.*, 2017, Vol. 252, P. 93–99.
25 Gibson I. R., Rehman I., Best S. M., Bonfield W., *J. Mat. Sci.: Mat. in Med.*, 2000, Vol. 11, P. 533–539.
24 Friederich R. J., Chappell H. F., Shepherd D. V., Best S. M., *J. R. Soc. Interface* [Electron. J.], 2015, Vol. 12, 20150190. URL: https://royalsocietypublishing.org/doi/pdf/10.1098/rsif.2015.0190 (accessed 10.05.2019).